# VALIDATION OF THE WIMS/PANTHER EMBEDDED SUPERCELL METHOD

**Paul Bryce[1], Glynn Hosking[2], Martin Knight[1], Ben Lindley[2], David Powney[2], Christophe Schneidesch[3], Nicolas Slosse[3] and Tom Taylor[1]**

[1]EDF Energy
Barnett Way, Barnwood, Gloucester, GL4 3RS, UK
[2]Wood Nuclear
Queen Mother Square, Poundbury, Dorset DT1 3BW, UK
[3]Tractebel Engineering S.A.
Boulevard Simon Bolivar 34, Brussels, Belgium

paul.bryce@edf-energy.com

## ABSTRACT

The WIMS/PANTHER Embedded Supercell Method (ESM) provides a significant improvement in prediction accuracy for radial power distributions for PWR reactors compared to the standard "two-step" approach, without the need for a significant increase in computational resource. Recent papers at PHYSOR conferences have outlined the details of the method and demonstrated its operation, and the accuracy improvements possible, by means of benchmarking calculations.

This paper applies the method to a 4-loop PWR in the U.K, and three PWRs (3-loop and 2-loop) in Belgium. Comparisons are made against measured data from the start-of-cycle physics testing performed for each cycle, and power-shape measurements collected during the cycle using a conventional "two-step" nodal reactor solution, and with the ESM. All results will be presented with the JEF2.2 nuclear data library, for ease of comparison between the methods and previously reported results, although the effects of more modern evaluations will be commented upon.

The benchmark calculations referred to above studied a challenging MOX/$UO_2$ benchmark core akin to an SMR. The four reactors studied here include conventional $UO_2$-only core designs and cycles with $UO_2$/MOX mixed cores. A variety of boron- and gadolinium-based burnable absorbers are also present. The data is used to show that the method both operates successfully for real reactor problems, and delivers improvements in the prediction accuracy of measured parameters.

KEYWORDS: WIMS, PANTHER, Core, Validation, Embedded

## 1. INTRODUCTION

This paper presents a summary of results comparing core calculations employing the WIMS/PANTHER Embedded Supercell Method (ESM) against plant measurements, for a range of operating PWRs.

The ESM is a recent development in the WIMS [1] and PANTHER [2] codes which is intended to provide a significant improvement in prediction accuracy in radial power distributions for PWR reactors compared to the standard "two-step" approach, without the need for a significant increase in computational resource.

The method described here will eventually replace the existing method currently in use for both UK and Belgian reactors, which was described in [3]. While originally designed to provide improved accuracy for $UO_2$/MOX mixed cores, the method is capable of also providing improved modelling throughout any core, including at the core edge/reflector interface and with inserted control rods.

## 2. OVERVIEW OF METHOD AND BENCHMARKING

The ESM provides a correction to the standard 2-group homogeneous assembly treatment of the reactor core, by using more detailed local methods. The standard treatment takes single assembly data from the lattice code in an idealised infinite environment. The embedded supercell methodology corrects this data to account for the actual environment in the core.

The method is aimed particularly at capturing the severe flux gradients across $UO_2$/MOX interfaces in PWR cores, but it is used at all interfaces including at the core edge.

In the demonstration route described here, a 6-group pin-by-pin diffusion calculation (using homogenised fuelpins) within PANTHER is used as the more detailed local method, but other methods could be used in principle.

The local problems are 2D supercells containing four quarter assemblies. Many of these problems will be needed to cover all the interfaces in a whole core problem, but each of them assumes zero current boundary conditions over the assembly mid-lines, and so are independent and can be run in parallel.

There are three broad stages in the use of the embedded supercell methodology: single assembly, supercell and whole core.

The initial stage is to establish the nuclear data libraries for the detailed pin-by-pin and standard smeared models for application to the embedded supercells. These *must* be fully consistent in the single assembly so that all subsequent differences in a supercell are due to the change in environment. To ensure this, the smeared model used for the supercells is derived directly from the PANTHER pin model in a single assembly environment.

The second stage, which is performed when the loading pattern for a cycle has been defined, is to list each supercell in the core and then evaluate them with both the detailed and the smeared models, in order to define corrections to the standard smeared model due to the change in environment. In particular corrections are derived for the cross-sections, discontinuity factors, pin powers and detector responses.

The third stage is to apply these supercell corrections in a whole core analysis of the fuel cycle (and optionally any assessment based on this, for example fault transients). The corrections are

applied on top of a calculation route which is otherwise an entirely standard "two-step" method. See [4] for more detail of the methodology.

### 2.1. Benchmarking of the Method

The method was demonstrated by solving supercells of fuel assemblies taken from the KAIST benchmark problem [5], and ultimately the KAIST core itself, which is a 2D small SMR-like core with an explicit steel baffle reflector, containing $UO_2$ and MOX fuel along with gadolinium poisons and control rods.

Supercell cases ranged from 2x2 chequerboards, 2x2 problems with depletion and refuelling and "line" supercells incorporating reflector boundaries. Solutions to the whole-core KAIST problem, including extensions for depletion and refuelling, have previously been published in [4], and further refined in [6].

### 2.2. Effects of the Embedded Corrections

When embedded corrections are applied to the whole-core models, correction parameters are applied to all the main two-group cross-sections, together with discontinuity factors, detector micro-cross-sections and pin power form factors.

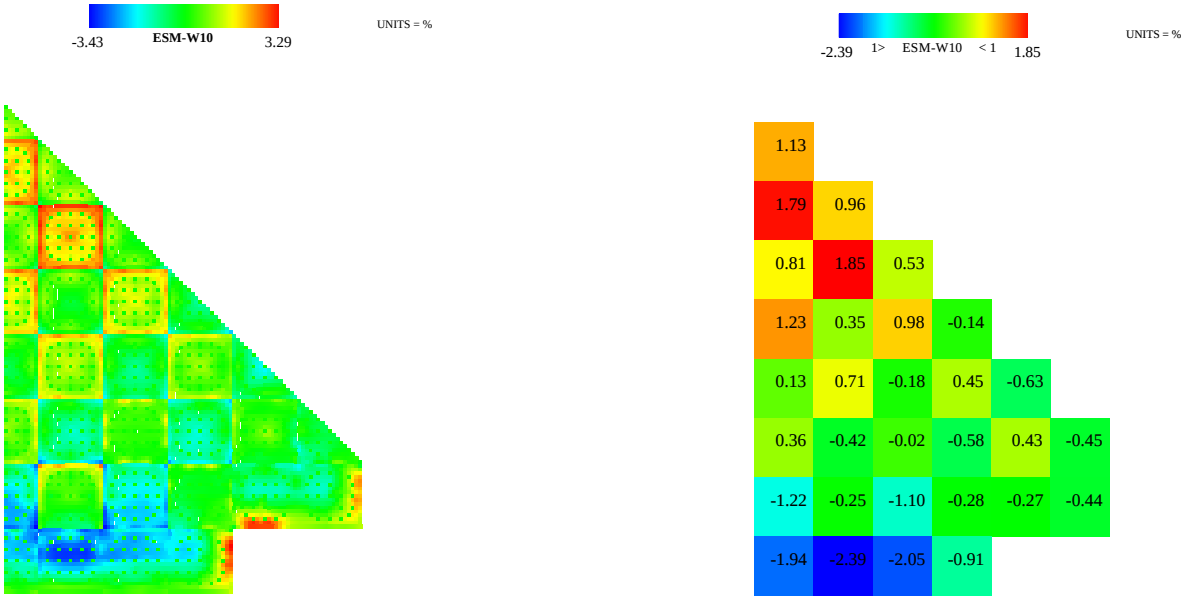


(a) Change in Pin Powers (b) Change in Detector Reaction Rate

**Figure 1: Example Pin Power and Detector Changes Introduced by the ESM**

To illustrate the effects of the corrections, figure 1 shows the impact of the ESM when applied

to a standard 4-loop PWR *. The reactor state is BOC1 at HZP with the control bank roughly $\frac{1}{4}$ inserted. The maps show the changes in reconstructed pin-powers (percentage relative to core average power) and detector reaction rates. Changes are particularly visible at assembly interfaces between poisoned and unpoisoned fuel, and around the core/reflector boundary; for this core, a small centre/edge power shift is also introduced. A core loaded with more challenging fuel such as MOX could show larger corrections (see [4,6]).

## 3. VALIDATION STATUS

### 3.1. Existing Approved Routes

In both UK and Belgium, current plant operation is underwritten by a calculation route run broadly as described in [3].

Since then additional capabilities have become available in both WIMS and PANTHER; in the former code developments in energy group representation and the use of a heterogeneous transport calculation (Method of Characteristics, MoC) for the assembly calculations; in the latter code the use of microscopic depletion and a switch to 4-nodes per assembly radially. Adoption of these set of options defines an modern "base" model.

The ESM can then be deployed on top of this model, and the results in the previous section illustrate the differences between the "base" model, and that using the ESM.

The current route in use in both countries utilises JEF2.2 since it was validated and endorsed close to the year 2000. Both base and ESM models continue to use JEF2.2 data in this paper so that the effects of the methodology developments can be more clearly seen.

Details of the various models are shown in table I.

The ESM method can be employed as an optional, additional model on top of the "W10" model shown above. The only difference is the use of a more recent PANTHER version (5.6.6) and reversion to a single-region of radial reflector data (since azimuthal differences are included via the explicit, heterogeneous model used in the ESM, rather than needing to be approximated by separate slab models in the lattice code.)

## 4. PLANT VALIDATION

The following section presents the results of comparisons performed on a selection of the plants from the UK and Belgian fleets:

- Plant A: is a 4-loop, 12 foot, 193 assembly, 3411 $\mathrm{MW}_{th}$ reactor in the UK. 17 cycles of 18-month length using $UO_2$ fuel covering enrichments between 2.1 and 4.6$^{\mathrm{w}}/_{\mathrm{o}}$, assembly burnups up to 52 $\mathrm{GWd/tU}$, and burnable poisons including discrete boron and integral gadolinium, from 4 to 8$^{\mathrm{w}}/_{\mathrm{o}}$.

*Here the reactor is the 4-loop Watts Bar unit 1 problem #5, as described in [7,8].

**Table I: Comparison of WIMS/PANTHER Models Applied**

| **Item** | **Code Route** | |
|---|---|---|
| | "in-use"/"LWRWIMS" | "base"/"W10" |
| Nuclear Library | JEF2.2 | JEF2.2 |
| Lattice Code | LWRWIMS5a | WIMS10 |
| Library Groups | 69 | 172 |
| Assembly Transport Method | Diffusion, with transport corrections | MoC |
| Transport Groups | 6 | 22 |
| Reactor Code | PANTHER 5.0 | PANTHER 5.6.x |
| Radial Refinement | 1x1 | 2x2 |
| Radial Reflector Treatment | 1-region (Plant A) or 2-region (B,C,D), Homogenized, Albedo-preserving | 2-region, Homogenized, Albedo-preserving |
| Axial Reflector Treatment | Implicit, Extrapolation Length (Plant A); as radial (plant B,C,D). | Explicit, Albedo-preserving |
| Depletion Method | Macroscopic+Spectral Index | Microscopic |
| Thermal Feedback | Single pin | Single pin |

- Plant B: is a 3-loop, 12 foot, 157 assembly, 2865 $MW_{th}$ (after power uprate) reactor in Belgium. Cycle lengths of between 12 and 16 months. Fuel characteristics similar to Plant A.
- Plant C: also 3-loop, 12 foot, 157 assemblies. Power (after update) is 3054 $MW_{th}$. Cycle lengths of between 12 and 16 months, some cycles included MOX. Fuel same/similar as plant A/B.
- Plant D: is a 2-loop, 8 foot, 121 assembly, 1311 $MW_{th}$ reactor, running a 12-month cycle, with no gadolinium poisons. For this reactor the model was initialised (based on previously recorded irradiations) at cycle 27 and results are presented from cycle 30 onwards.

### 4.1. Critical Boron Concentrations at BOC

Figure 2 shows the Calculated minus Measured (C−M) prediction accuracy of the initial critical boron concentration at start of cycle. WIMS10-based models are seen to provide more consistent cycle-to-cycle behaviour than the original LWRWIMS models; the reactivity difference introduced by the ESM method is less than 10 $\mathrm{ppm}$ and broadly cycle-independent (larger differences are seen in MOX cycles).

For plant A, minor fuel design changes were made at cycles 5, 10 with a change from natural to reprocessed uranium (containing elevated levels of $^{234}\mathrm{U}$ and $^{236}\mathrm{U}$) occurring at cycle 11.

### 4.2. Isothermal Temperature Coefficients

Figure 3 shows the C−M prediction accuracy of the isothermal temperature coefficients at zero power, start of cycle, evaluated at the calculated boron concentrations. The large improvement in systematic bias for WIMS10-based models comes partly from the enhanced energy group structure used in the WIMS calculations, and partly from the use of microscopic depletion in PANTHER.

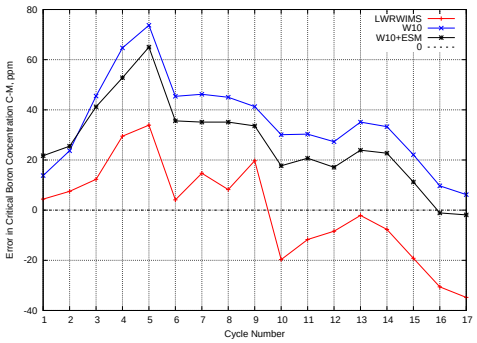


(a) Plant A

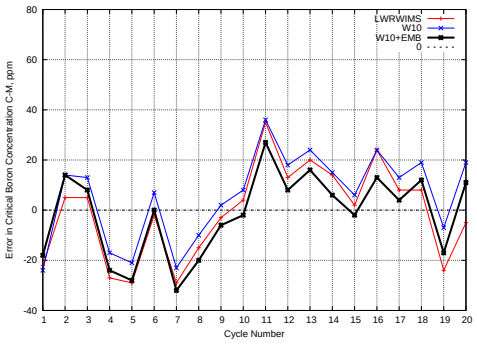


(b) Plant B

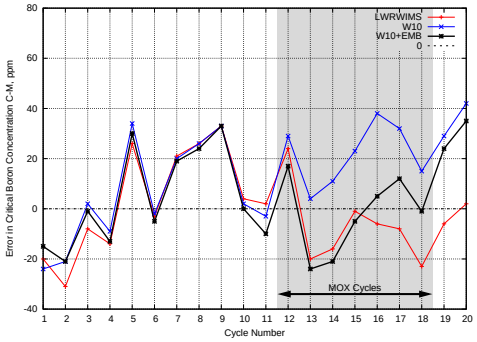


(c) Plant C

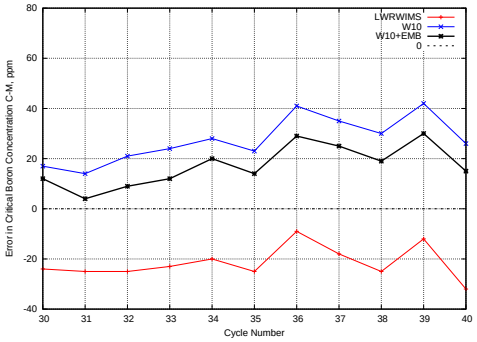


(d) Plant D

**Figure 2: Critical Boron Concentrations at BOC, HZP**

### 4.3. Control Rod Worths

Figure 4 and table II shows the C−M prediction accuracy of the control bank worths as measured at start of cycle. The scatter is reduced by the WIMS10-based model and, for some plants, improved further with the ESM.

**Table II: Percentage Errors in Prediction of Control Rod Bank Worth Measurements**

| Plant | N | LWRWIMS | W10 | W10+ESM |
|---|---|---|---|---|
| Plant A | 129 | $2.6 \pm 7.2$ | $-0.3 \pm 4.8$ | $-1.7 \pm 5.6$ |
| Plant B | 29 | $-0.5 \pm 5.5$ | $-0.7 \pm 5.0$ | $+0.3 \pm 4.8$ |
| Plant C | 51 | $+0.8 \pm 4.5$ | $-0.9 \pm 4.4$ | $+0.4 \pm 4.1$ |
| Plant D | 44 | $-1.6 \pm 3.2$ | $-2.6 \pm 2.5$ | $-0.5 \pm 2.4$ |

For plant A, measurements were made via boron dilution and rod swap in cycles 1–3, and dynamic measurements from cycle 4 onwards. Measurements in cycle 8 are believed to be biased due to equipment electrical setup.

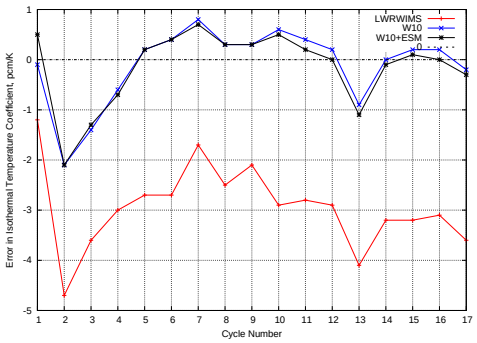


(a) Plant A

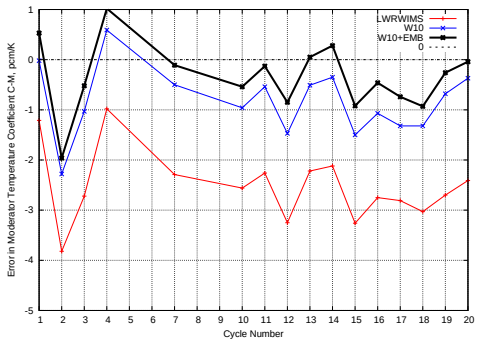


(b) Plant B

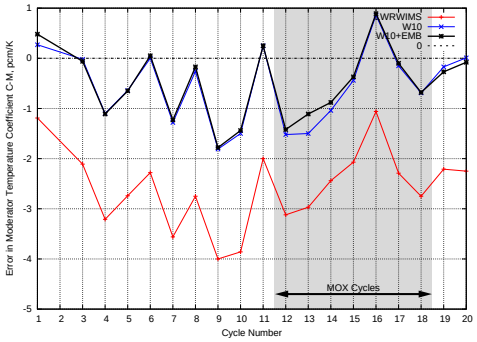


(c) Plant C

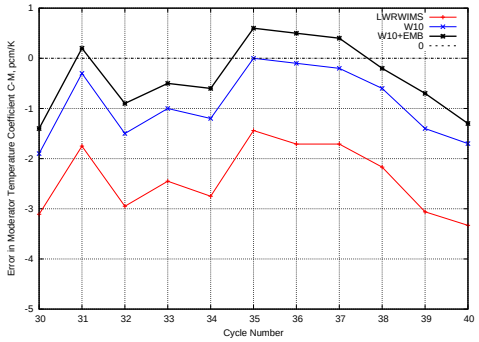


(d) Plant D

**Figure 3: Isothermal Temperature Coefficients at BOC, HZP**

### 4.4. Through-Cycle Radial Power Shape

Figure 5 shows a comparison between the radial powershape accuracy of the various models as compared to axially-integrated measured reaction rates in at-power equilibrium flux maps. For 4–5 representative maps per fuel cycle, the RMS error over the ≈50 instrumented locations is calculated and this is presented as a time sequence.

Table III shows the overall 2D statistics through the lifetime of the plants. For plant A, all three models show broadly similar accuracies, but note that the W10 model has a radial reflector model which uses separate, manually created data for the "flat edge" and "corner" regions, while the ESM model incorporates this azimuthal dependence automatically.

In some cases the "W10" results are slightly inferior to those with the older LWRWIMS model; this is due to WIMS10 predicting a slightly different fast radial diffusion coefficient in the core. A companion paper in this conference [9] shows that the WIMS10 diffusion coefficient, when combined with a suitable whole-core transport solution can produce a core power shape consistent with a continuous energy Monte-Carlo calculation.

For all plants the ESM improves comparison with measurements, both in the MOX-specific cycles and overall. Note that the calculated detector response only accounts for neutron-induced response,

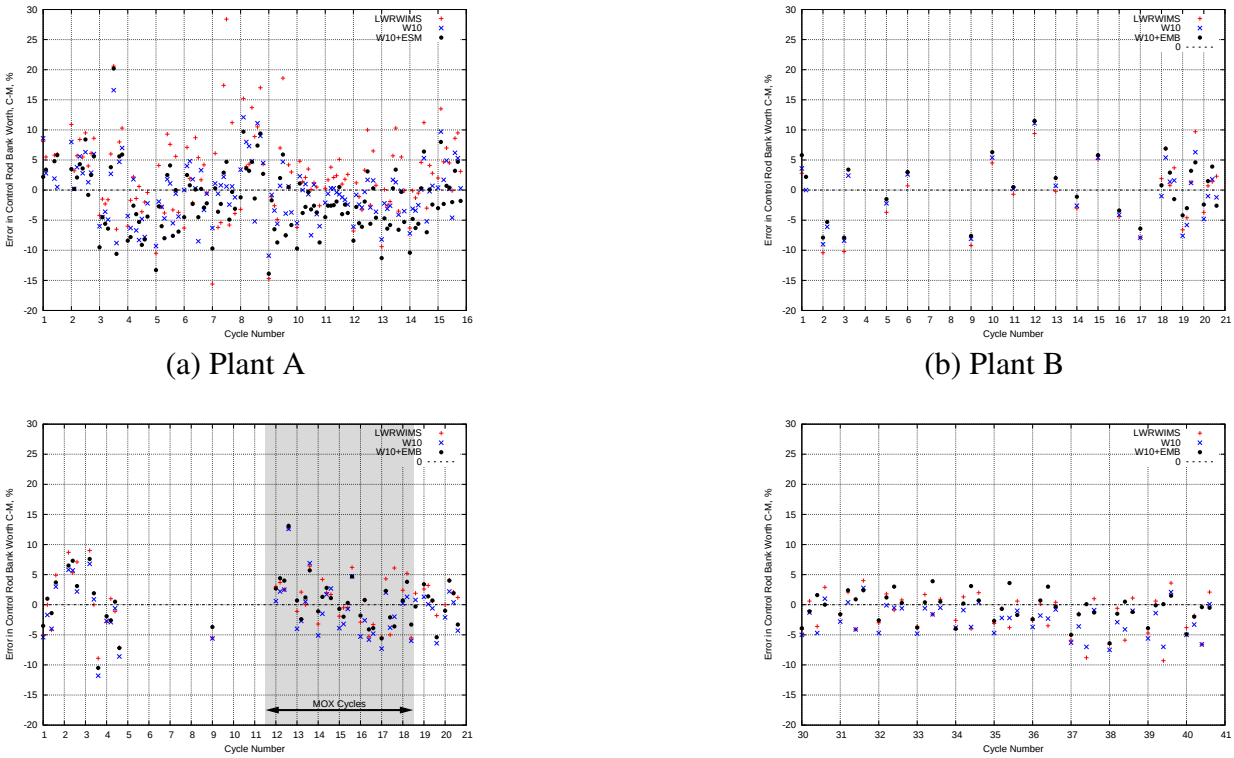


(a) Plant A

(b) Plant B

(c) Plant C

(d) Plant D

**Figure 4: Individual Control Rod Bank Worths at BOC, HZP**

no account has been taken of sensitivity of the detector to gamma flux; accounting for this may offer further improvements in prediction accuracy.

**Table III: Percentage RMS Error in Prediction of Axially Integrated Reaction Rates**

| Plant | $N_{map}$ | $N_{scan}$ | LWRWIMS | W10 | W10+ESM |
|---|---|---|---|---|---|
| Plant A | 77 | 4295 | 1.63 | 1.62 | 1.48 |
| Plant B | 103 | 5150 | 1.51 | 1.78 | 1.46 |
| Plant C (MOX cycle) | 36 | 1800 | 2.63 | 2.40 | 2.26 |
| Plant C (all) | 101 | 5050 | 1.95 | 1.97 | 1.79 |
| Plant D | ≈120 | ≈3600 | 1.67 | 1.87 | 1.41 |

Figure 6 shows an example from plant A of the 2D reaction rate errors plotted as a function of assembly burnup. Very little bias is seen, e.g. for the high-burnup fuel assemblies.

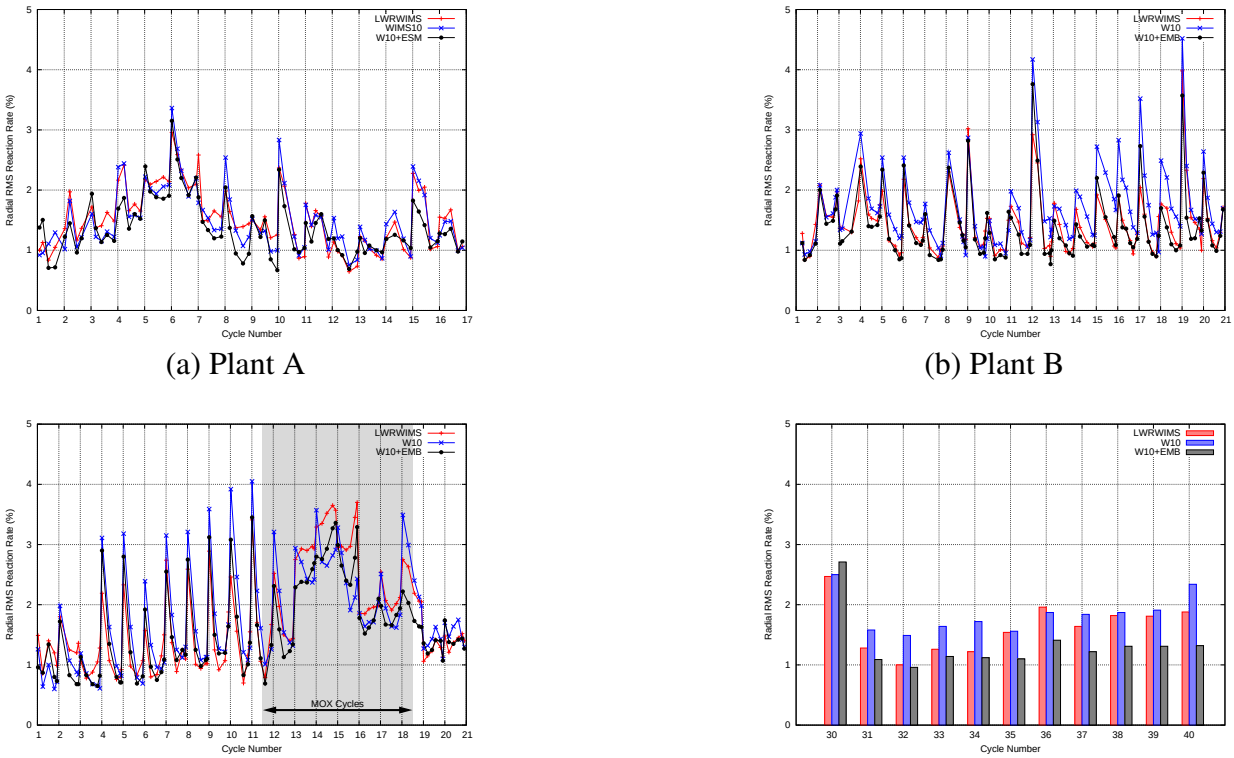


(a) Plant A

(b) Plant B

(c) Plant C

(d) Plant D

**Figure 5: RMS Radial Powershape error as a function of time; Full Power Maps**

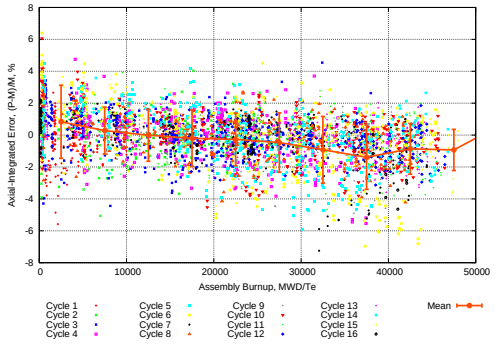


(a) Plant A

**Figure 6: Radial Powershape error as a function of Assembly Burnup**

## 4.5. Through-Cycle Reactivity

The effects of the three models on reactivity through the fuel cycles were evaluated for Plant A. These showed, in general, the same features (model-to-model) as seen in the start-of-cycle reactivity comparisons, see section 4.1.

There is considerable uncertainty in these data, due to the need to model and compensate for the depletion of $^{10}$B in the coolant. Nonetheless the suggestion is that a bias remains between beginning and end of cycle, which is reduced in the WIMS10-based models but remains of the order of $-30$ppm over an 18 month (500 day) cycle.

### 4.6. Summary of Plant Comparisons

Comparisons against plant data show that the new model, utilising WIMS10 data and the ESM technique, performs as well as, or better than, the existing models when applied to the UK and Belgian fleets.

### 4.7. Impact of later Data Libraries

A limited re-evaluation of these results has been performed using JEFF3.1.2 data.

When comparing JEF2.2 and JEFF3.1.2 with the same calculational methods, very little difference is observed in core radial and axial powershape. However a significant reduction in predicted core reactivity is seen, of order $-80$ppm for the HZP boron measurement at equilibrium core burnups (a smaller reduction at lower burnups, e.g. $-40$ppm at start-of-life).

## 5. CONCLUSIONS

This paper checks the accuracy of the WIMS10/PANTHER Embedded Supercell Method (ESM) against a subset of plant validation data available from UK and Belgian PWRs.

The ESM has previously been shown, via benchmarking calculations, to give a significant increase in fidelity for pin-power distributions when compared against reference transport calculations. In this paper, the method (and other improvements relating to the use of the modern WIMS10 code) are compared against real plant data.

Generally results using the newer models are similar to or better than the in-use production models and are improved for $UO_2$/MOX cycles, which was the original motivation for the development of the method. Significant improvements in accuracy are seen in the prediction of ITC, where the long-standing negative bias seen in [3] is eliminated due to a combination of more detailed energy group structures in the WIMS calculations, combined with microscopic depletion.

When combined with the conclusions from the earlier benchmarking studies (whose effects are dominated by changes at assembly interfaces, and therefore not always visible at the central detector locations) these conclusions make a powerful argument for the adoption of the modern methods.

Future work will extend the benchmarking of the method to comparisons with whole-core Monte-Carlo calculations, and plant validation to all UK and Belgian reactors with modern nuclear datasets.

## REFERENCES

[1] B. A. Lindley, T. D. Newton, J. G. Hosking, P. N. Smith, D. J. Powney, B. Tollit, and P. J. Smith. "Release of WIMS10: A Versatile Reactor Physics Code for Thermal and Fast Systems." In *Proceedings of ICAPP 2015, Nice, France* (May 2015).

[2] P. K. Hutt, N. Gaines, M. McEllin, R. J. White, and M. J. Halsall. "The UK Core Performance Code Package." *Nuclear Energy*, **volume 30, No.5**, pp. 291–298 (1991).

[3] J. L. Hutton, D. J. Powney, P. K. Hutt, M. P. Knight, P. Bryce, A. Goddard, C. R. Schneidesch, D. Vantroyen, S. Bosso, and O. Ergo. "Comparison of WIMS/PANTHER Calculations with Measurement on a Range of Operating PWR." In *Transactions of International Topical Meeting on Advances in Reactor Physics and Mathematics and Computation into the Next Millennium, PHYSOR 2000*. American Nuclear Society, Pittsburgh (May 2000).

[4] M. Knight, P. Bryce, and S. Hall. "WIMS/PANTHER analysis of UO2/MOX cores using embedded supercells." *Nuclear Technology*, **volume 183**(3), pp. 398–408 (2013).

[5] N. Z. Cho. "KAIST/NurapT: Benchmark Problem 1A: MOX Fuel-Loaded Small PWR Core (MOX Fuel with Zoning)." (2000). URL http://nurapt.kaist.ac.kr/benchmark.

[6] M. Knight, P. Bryce, and T. Taylor. "Use of a Line of Pincells to Refine Discontinuity Factors and Group Structure for MOX/UO2 Modelling in the Embedded Supercell Methodology." In *Topical Meeting on Reactor Physics, PHYSOR 2016, Sun Valley, Idaho, USA*. American Nuclear Society (April 2016).

[7] A. T. Godfrey. "VERA Core Physics Benchmark Progression: Problem Speifications." Technical Report CASL-U-2012-0131-004, CASL (Revision 4, August 2014).

[8] J. C. Gehin, A. T. Godfrey, F. Franceschini, T. M. Evans, B. S. Collins, and S. P. Hamilton. "Operational Reactor Model Demonstration with VERA: Watts Bar Unit 1 Cycle 1 Zero Power Physics Tests." Technical Report CASL-U-2013-0105-001, CASL (Revision 1, August 2013).

[9] T. Taylor, M. Knight, and P. Bryce. "Use of the simplified PN equations and transport corrections in the WIMS/PANTHER Embedded Supercell Method." In *PHYSOR2020: Transition to a Scalable Nuclear Future, Cambridge UK*. American Nuclear Society (April 2020).